Available online at www.sciencedirect.com
ScienceDirect
Journal of Solid State Chemistry 179 (2006) 3505–3510
JOURNAL OF SOLID STATE CHEMISTRY
www.elsevier.com/locate/jssc

High-temperature neutron diffraction study of the cation ordered perovskites $TbBaMn_2O_{5+x}$ and $TbBaMn_2O_{5.5-y}$

Elizabeth Castillo-Martínez[a], Anthony J. Williams[b], J. Paul Attfield[b,*]

[a]Dpto. de Quimica Inorganica I, Facultad de Ciencias Quimicas, Universidad Complutense, Av. Complutense s/n, 28040 Madrid, España
[b]Centre for Science at Extreme Conditions and School of Chemistry, University of Edinburgh, King's Buildings, Mayfield Road, Edinburgh EH9 3JZ, United Kingdom

Received 26 May 2006; received in revised form 12 July 2006; accepted 16 July 2006
Available online 21 July 2006

Dedicated to Prof. H. Fuess on the occasion of his 65th birthday

Abstract

The miscibility of $TbBaMn_2O_{5+x}$ and $TbBaMn_2O_{5.5-y}$ has been investigated at 100–600 °C using in situ powder neutron diffraction. No miscibility is observed, and the two phases remain oxygen stoichiometric ($x, y = 0$) at 600 °C. Structure refinement results show that neither material undergoes a phase transition in this temperature range. $TbBaMn_2O_5$ is Mn^{2+}/Mn^{3+} charge ordered and any charge melting transition is >600 °C. This symmetry-broken charge ordering is remarkably robust in comparison to that in other oxides.

Keywords: Neutron diffraction

1. Introduction

Since the discovery of the colossal magnetoresistance (CMR) effect in manganese oxide perovskites $Ln_{1-x}M_xMnO_3$ (Ln = trivalent lanthanide, M = Ca, Sr or Ba), these materials have been extensively studied with a view towards better understanding and improving their properties. Over the past decade, a particular class of 50% doped manganites, in which the A-site Ln^{3+} and Ba^{2+} cations order in alternating [001] perovskite layers, have been of interest. The first example of such an ordered perovskite was $YBaMn_2O_5$ [1] in which the oxygen sites in the Y layers are vacant, reducing the yttrium coordination to 8. The manganese–oxygen network consists of double layers of MnO_5 square pyramids linked through all their apices. Subsequent neutron diffraction studies on $YBaMn_2O_5$ [2], and the lanthanum analogue $LaBaMn_2O_5$ [3], showed it to have a tetragonal $\sqrt{2}a_p \times \sqrt{2}a_p \times 2a_p$ $P4/nmm$ symmetry cell, with a "rocksalt" type ordering of Mn^{2+} and Mn^{3+} valences.

Oxygen can be intercalated into the La layer of $LaBaMn_2O_5$ to yield first $LaBaMn_2O_{5.5}$ [4] and then $LaBaMn_2O_6$ [3], without disturbing the La/Ba order. The ordered form of $LaBaMn_2O_6$ has tetragonal $a_p \times a_p \times 2a_p$ $P4/mmm$ symmetry, while the cation disordered form is cubic. Both materials are ferromagnetic metals; however, the introduction of an ordering between the A-site cations increases the Curie temperature from 270 K for the disordered phase to 335 K for the ordered one.

For all large Ln = La–Nd, there is no evidence for a charge ordering of Mn^{3+} and Mn^{4+} ions in the structure. For small Ln = Y, Sm–Ho, however, the internal strains imposed by the A-cation ordering of mismatched layers leads to the stabilisation of novel charge and orbitally ordered structures [5–8] in $LnBaMn_2O_6$, including a "rocksalt" type ordering of Mn^{3+} and Mn^{4+} charge states in $YBaMn_2O_6$ and $TbBaMn_2O_6$, which has been shown [9] to persist to high temperatures (498 and 473 K, respectively). The structure of the oxygenated intermediate phase $YBaMn_2O_{5.5}$ has recently been reported [10] $YBaMn_2O_{5.5}$ has a distorted variant of the $LaBaMn_2O_{5.5}$ structure, with an orthorhombic $Icma$ cell in which the Mn polyhedra are tilted around the [001] axis.

*Corresponding author. Fax: +44 131 651 4743.
E-mail address: j.p.attfield@ed.ac.uk (J.P. Attfield).

0022-4596/$ - see front matter © 2006 Elsevier Inc. All rights reserved.
doi:10.1016/j.jssc.2006.07.019

One of the most notable aspects of this series of structures is that, for small *Ln*, Mn^{3+}/Mn^{4+} ordered $LnBaMn_2O_6$ results from topotactic oxygen intercalation into Mn^{2+}/Mn^{3+} ordered $LnBaMn_2O_5$ (Fig. 1). Charge ordering in such a layered host and its intercalated product is unprecedented, and leads to the question of whether the intercalation reactions are *topoelectronic* i.e. whether any charge-ordering memory effects are possible, during the oxygen intercalation, on either an atomic or domain scale.

For the reaction to be topoelectronic would require a continuous structural transformation from $LnBaMn_2O_5$ to $LnBaMn_2O_6$. In this study of the first oxygenation step, we have investigated the structural evolution between $TbBaMn_2O_5$ and the intermediate oxygen intercalation product $TbBaMn_2O_{5.5}$. The miscibility of these phases has been investigated by *in situ* neutron diffraction up to a temperature of 600 °C.

2. Experimental

To prepare a sample of intermediate oxygen content near $TbBaMn_2O_{5.25}$, a solid state reaction was performed under moderately reducing conditions, using pelleted high-purity Tb_4O_7, $BaCO_3$ and Mn_2O_3 as the starting materials. The reaction was conducted in a tube furnace under an argon flow (99.999%) at 1400 °C for two periods of 12 h, with intermediate regrinding and repelleting. The sample was cooled to room temperature at 5 °C/min after the final heating. The oxygen content was estimated from the weight changes during reaction, and the more precise analysis from the neutron study below shows that the bulk composition was fortuitously close to 5.25.

Powder neutron diffraction data were collected from the high resolution powder diffractometer (HRPD) instrument at the ISIS spallation facility, UK using a standard ISIS furnace with vanadium elements and shields. The sample was sealed in a cylindrical, 8 mm diameter, vanadium can within the evacuated furnace. Scans of approximately 1.5 h each were collected at 100 °C intervals between 100 and 600 °C. Profiles from the backscattering ($2\theta = 168°$) and the $2\theta = 90°$ detector banks were simultaneously Rietveld analysed using the general structure analysis system (GSAS) programme [11] The background scatter was fitted by linear interpolation and the peak shapes were modelled by a standard convolution of exponential and pseudo-Voigt functions.

3. Results

Attempts to fit any of the patterns using a single phase model were unsuccessful. Excellent fits were obtained at all temperatures using a mixture of $TbBaMn_2O_{5+x}$ and $TbBaMn_2O_{5.5-y}$ phases (see Fig. 2), giving χ^2 values 3.94–4.50. Each phase was well fitted by the model previously observed for the yttrium analogue, with orthorhombic *Icma* symmetry for $TbBaMn_2O_{5.5-y}$ [10], and tetragonal *P*4/*nmm* symmetry for $TbBaMn_2O_{5+x}$ [2]. Fractional occupancies for the oxygen positions within the Tb layers were initially refined, and the values were subsequently fixed to be 0 or 1 when no significant deviation was found. No significant correlations between the parameters for the two phases were observed during refinement, reflecting the high $\Delta d/d$ resolution of the neutron data. Refined lattice and structural parameters are given in Tables 1 and 2. The overall sample oxygen content was calculated from the oxygen site occupancies and phase fractions (Table 3).

The Mn–O distances in the two structures are shown in Table 4 and the thermal evolutions of the bond lengths in $TbBaMn_2O_{5+x}$ are shown in Fig. 3. Bond Valence Sums (BVS) around the Mn sites are calculated using standard parameters for Mn^{2+} and Mn^{3+} [12], enabling the linearly

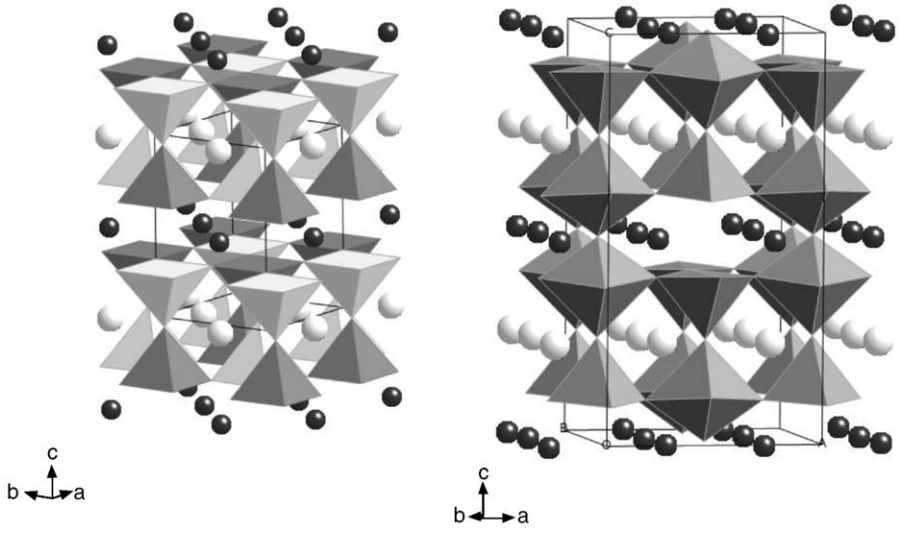

Fig. 1. The structures of (a) $TbBaMn_2O_5$ (with the $Mn^{2+}O_5$ and $Mn^{3+}O_5$ square pyramids shaded differently) and (b) $TbBaMn_2O_{5.5}$. Tb and Ba atoms are represented by black and white spheres, respectively.

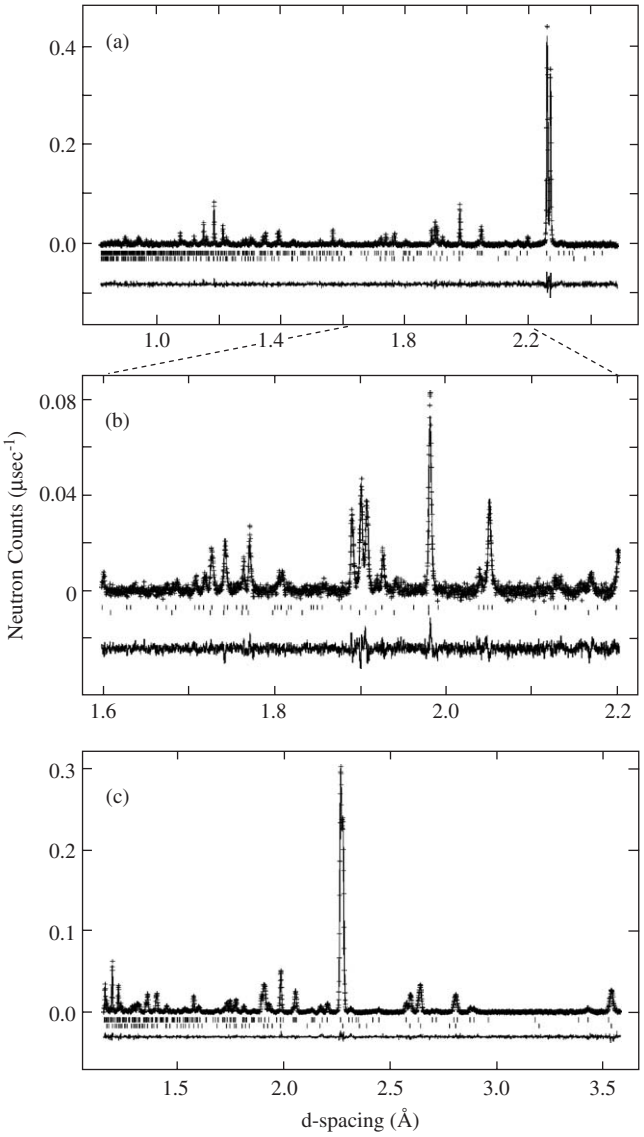

Fig. 2. The 600 °C neutron powder diffraction profiles for the sample consisting of $TbBaMn_2O_5$ (lower markers) and $TbBaMn_2O_{5.5}$ (upper markers); (a) fitted backscattering ($2\theta = 168°$) profile, part of which is expanded in (b); (c) fitted $2\theta = 90°$ bank data.

interpolated valences and the degree of charge order (%CO) in $TbBaMn_2O_{5+x}$ to be estimated using the formulae [13] shown in Table 4. The standard deviations in the bond distances lead to errors of $\pm 3\%$ in the BVS's, and hence uncertainties of ± 10 in the %CO for $TbBaMn_2O_{5+x}$.

4. Discussion

The high resolution neutron data provide precise estimates of oxygen site occupancies in the two phases. However, the results in Table 3 show that there is no evidence of oxygen miscibility between $TbBaMn_2O_{5+x}$ and $TbBaMn_2O_{5.5-y}$ up to 600 °C. Although these phases, respectively, show a small oxygen excess and deficiency at low temperatures (x, $y \approx 0.02$), these are lost as the samples equilibrate above 300 °C (Table 3). The oxygen contents at low temperatures are thus non-equilibrium values that may have resulted from the relatively rapid cooling of the sample after synthesis. The overall oxygen content of the sample remains constant to 600 °C, showing that there was no loss of gaseous oxygen from the sample can during the experiment. It is evident that much higher temperatures will have used to establish whether the miscibility gap between $TbBaMn_2O_{5+x}$ and $TbBaMn_2O_{5.5-y}$ can be closed.

Although the main aim of this experiment was not realised, the neutron data provide good-quality refinements of the $TbBaMn_2O_{5+x}$ (Table 1) and $TbBaMn_2O_{5.5-y}$ (Table 2) structures up to 600 °C. Neither material shows a phase transition or any structural anomalies in this range. $TbBaMn_2O_{5.5}$ contains Mn^{3+} in both 5-coordinate square pyramidal and 6-coordinate octahedral sites. This is supported by the calculated BVS for the two Mn sites which show only small discrepancies from the ideal value of 3. Some oxygen disorder is frozen in from the high temperature synthesis, with significant oxygen vacancies at the O5 sites, and a smaller excess at the O6 positions, but

Table 1
Refined lattice parameters, coordinates, partial occupancies and isotropic thermal parameters U_{iso}'s (Å^2) for $TbBaMn_2O_{5+x}$ at 100–600 °C in space group $P4/nmm$ with atoms in the following positions: Tb, 2b ($\frac{3}{4},\frac{1}{4},\frac{1}{2}$); Ba, 2$a$ ($\frac{3}{4},\frac{1}{4},0$); Mn1 ($Mn^{2+}$), 2$c$ ($\frac{1}{4},\frac{1}{4},z$); Mn2 ($Mn^{3+}$), 2$c$ ($\frac{1}{4},\frac{1}{4},z$); O1, 8j ($x,x,z$); O2, 2$c$ ($\frac{1}{4},\frac{1}{4},z$); O3, 2$c$ ($\frac{1}{4},\frac{1}{4},\frac{1}{2}$)

	T (°C)	100	200	300	400	500	600
	a (Å)	5.56924(8)	5.57459(8)	5.58051(9)	5.58656(9)	5.59250(9)	5.59848(9)
	c (Å)	7.67808(11)	7.69364(11)	7.70996(13)	7.72548(13)	7.74112(13)	7.75787(14)
Tb	U_{iso}	0.0015(4)	0.0014(4)	0.0035(4)	0.0039(5)	0.0043(5)	0.0071(5)
Ba	U_{iso}	0.0043(4)	0.0062(5)	0.0058(5)	0.0123(6)	0.0153(6)	0.0191(6)
Mn1	z	−0.2536(4)	−0.2544(4)	−0.2506(4)	−0.2517(4)	−0.2478(4)	−0.2464(4)
Mn2	z	0.2784(4)	0.2761(4)	0.2788(4)	0.2747(5)	0.2769(5)	0.2763(4)
	U_{iso}(Mn)	0.0024(4)	0.0045(4)	0.0058(4)	0.0088(5)	0.0095(5)	0.0135(5)
O1	x	0.4914(2)	0.4916(2)	0.4915(2)	0.4904(2)	0.4906(2)	0.4921(2)
	z	0.31383(6)	0.31328(6)	0.31325(7)	0.31311(7)	0.31305(7)	0.31274(7)
O2	z	0.0106(4)	0.31328(6)	0.0066(4)	0.0071(5)	0.0060(5)	0.0071(5)
O3	occ	0.025(2)	0.014(2)	0.005(2)	0	0	0
	U_{iso}(O)	0.0074(3)	0.0088(3)	0.0120(4)	0.0130(5)	0.0161(5)	0.0202(5)

U_{iso}'s for the Mn sites, and for the O sites, were constrained to be equal.

Table 2
Refined lattice parameters, coordinates, partial occupancies and isotropic thermal parameters U_{iso}'s (Å^2) for $TbBaMn_2O_{5.5-y}$ at 100–600 °C in space group *Icma* with atoms in the following positions: Tb, 8*j* (*x*, 0, *z*); Ba, 8*j* (*x*, 0, *z*); Mn1, 8*f* (0, 1/4, z); Mn2, 8*f* (0, 1/4, *z*); O1, 16*k* (*x*, *y*, *z*); O2, 8*f* (0, 1/4, *z*); O3, 8*f* (*x*, 0, *z*); O4, 8*j* (*x*, 0, *z*); O5, 4*b* (0, 1/4, 1/2); O6, 4*a* (0, 1/4, 0)

	T (°C)	100	200	300	400	500	600
	a (Å)	8.1552(1)	8.1624(1)	8.1706(1)	8.1784(1)	8.1860(2)	8.1930(2)
	b (Å)	7.5750(1)	7.5833(1)	7.5928(1)	7.6025(1)	7.6126(1)	7.6246(1)
	c (Å)	15.3072(2)	15.3253(2)	15.3446(3)	15.3633(3)	15.3816(3)	15.3999(3)
Tb	*x*	0.2731(1)	0.2725(2)	0.2717(2)	0.2722(2)	0.2711(2)	0.2703(2)
	z	0.0038(1)	0.0040(1)	0.004(1)	0.0029(2)	0.0030(2)	0.0028(2)
	U_{iso}	0.0040(5)	0.0034(5)	0.0070(6)	0.0080(6)	0.0081(6)	0.0145(6)
Ba	*x*	0.2530(6)	0.2511(6)	0.2513(7)	0.2540(8)	0.2536(8)	0.2525(10)
	z	0.2499(2)	0.2510(2)	0.2494(2)	0.2514(3)	0.2520(3)	0.2521(3)
	U_{iso}	0.0067(6)	0.0057(6)	0.0073(6)	0.0069(7)	0.0054(7)	0.0096(7)
Mn1	*z*	0.1152(1)	0.1158(1)	0.1160(1)	0.1161(2)	0.1158(2)	0.1155(2)
Mn2	*z*	0.3759(2)	0.3767(2)	0.3766(2)	0.3770(2)	0.3771(2)	0.3770(2)
	U_{iso} (Mn)	0.0051(4)	0.0044(4)	0.0067(4)	0.0085(5)	0.0108(5)	0.0124(5)
O1	*x*	0.2305(2)	0.2304(2)	0.2306(2)	0.2300(2)	0.2300(2)	0.2293(2)
	y	0.2748(1)	0.2740(2)	0.2720(2)	0.2706(2)	0.2681(2)	0.2654(2)
	z	0.10042(6)	0.10051(6)	0.10040(7)	0.10071(7)	0.10051(7)	0.10075(7)
O2	*z*	0.2517(1)	0.2522(1)	0.2527(1)	0.2528(1)	0.2533(1)	0.2540(2)
O3	*x*	0.0310(2)	0.0297(3)	0.0297(3)	0.0265(3)	0.0264(3)	0.0233(4)
	z	0.0932(1)	0.0934(1)	0.0933(1)	0.0933(1)	0.0928(1)	0.0922(1)
O4	*x*	−0.0230(3)	−0.0224(3)	−0.0209(3)	−0.0187(3)	−0.0170(4)	−0.0154(4)
	z	0.3841(1)	0.3845(1)	0.3844(1)	0.3851(1)	0.3848(1)	0.3849(1)
O5	occ	0.930(5)	0.967(5)	0.987(6)	0.970(6)	1	1
O6	occ	0.020(5)	0.008(5)	0.009(5)	0.017(6)	0	0
	U_{iso}(O)	0.0091(3)	0.0109(3)	0.0137(4)	0.0154(4)	0.0185(4)	0.0219(4)

U_{iso}'s for the Mn sites, and for the O sites, were constrained to be equal.

Table 3
Refined phase fractions of $TbBaMn_2O_{5+x}$ and $TbBaMn_2O_{5.5-y}$ at 100–600 °C, and weighted total oxygen content per formula unit

T (°C)	$TbBaMn_2O_{5+x}$		$TbBaMn_2O_{5.5-y}$		Total O
	x	Fraction (%)	*y*	Fraction (%)	
100	0.025(2)	46.7(1)	0.021(2)	53.3(1)	5.27(1)
200	0.014(2)	47.3(1)	0.014(2)	52.7(1)	5.26(1)
300	0.005(2)	47.3(1)	0.004(2)	52.7(1)	5.26(1)
400	0	47.3(1)	0.007(2)	52.7(1)	5.26(1)
500	0	47.8(1)	0	52.2(1)	5.26(1)
600	0	49.2(1)	0	50.8(1)	5.25(1)

these deviations are annealed out above 400 °C in the present heating cycle.

$TbBaMn_2O_5$ contains 5-coordinate square pyramidal Mn sites, however the presence of two distinct positions results from Mn^{2+}/Mn^{3+} charge order, as is observed in $YBaMn_2O_5$ [2] and $LaBaMn_2O_5$ [3] The average Mn–O distances and the BVSs for the two sites change little with temperature, however, the individual bond lengths (Fig. 3) show marked changes as a consequence of the lattice connectivity (Fig. 1a) and the differing thermal expansions of the various cations. Ba^{2+} is the largest cation present and shows the largest increase in vibrational amplitude upon heating. The root mean square displacement $\sqrt{U_{iso}}$ for Ba (Table 1) increases from 0.07 Å at 100 °C to 0.14 Å at 600 °C. The Ba vibrations tend to make the surrounding MnO_3 cage more cubic with increasing temperature; the ratio of the Mn–Mn distance in the *c*-direction to that in the *ab* plane decreases from 4.085/3.938 Å = 1.037 at 100 °C to 4.055/3.959 Å = 1.024 at 600 °C. This leads to a decrease in the apical Mn1(Mn^{2+})–O2 bond length with increasing temperature (Fig. 3), while the other bonds show a gradual expansion.

BVS's for the two Mn sites in $TbBaMn_2O_5$ (Table 4) reveal clear evidence for substantial Mn^{2+}/Mn^{3+} charge ordering at all temperatures. The estimated charge separation is ~70% of the ideal value up to 500 °C, and the decrease to 62% at 600 °C may indicate the onset of charge melting. $TbBaMn_2O_5$ is a symmetry-broken charge ordered oxide, as the translational symmetry between the two Mn sites is broken by the CO, and the consequent lattice distortions. A recent review [13] of symmetry-broken CO

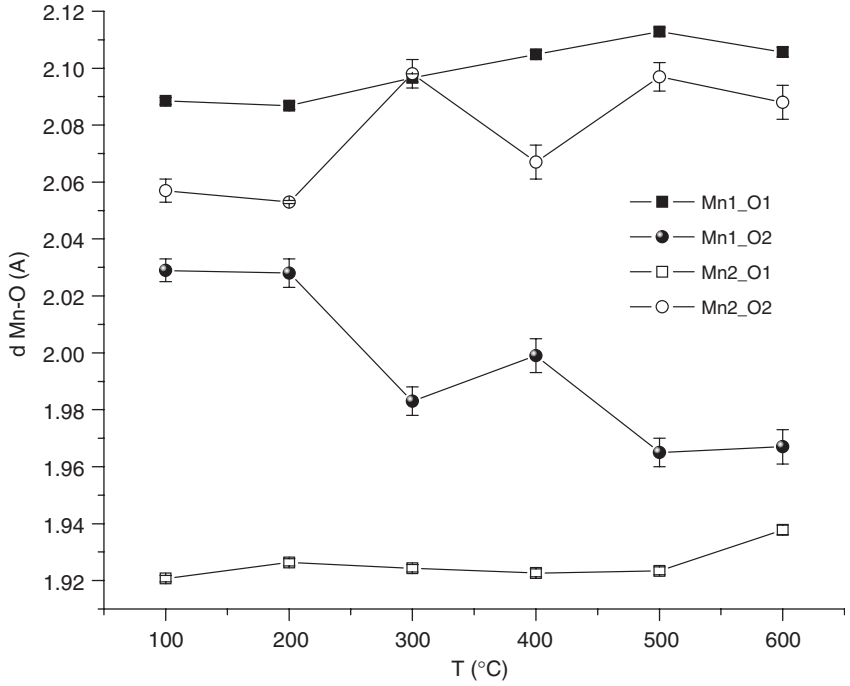

Fig. 3. Thermal evolution of the Mn–O distances around the two Mn sites in $TbBaMn_2O_{5+x}$.

Table 4
Temperature variation of the Mn–O distances (Å), bond valence sums (V)[a] for $TbBaMn_2O_{5+x}$ and $TbBaMn_2O_{5.5-y}$, and the degree of charge order (%CO) in $TbBaMn_2O_{5+x}$[b]

Phase	Bond	Temperature (°C)					
		100 °C	200 °C	300 °C	400 °C	500 °C	600 °C
$TbBaMn_2O_{5+x}$							
4 ×	Mn1–O1	2.089(1)	2.087(1)	2.097(1)	2.105(2)	2.113(2)	2.106(2)
1 ×	Mn1–O2	2.029(4)	2.028(5)	1.983(5)	1.999(6)	1.965(5)	1.967(6)
occ ×	Mn1–O3	1.892(3)	1.890(3)	1.923(3)			
	<Mn–O>	2.076(2)	2.074(2)	2.074(3)	2.084(3)	2.083(3)	2.078(3)
	V	2.28	2.28	2.29	2.24	2.25	2.27
4 ×	Mn2–O1	1.921(1)	1.926(1)	1.924(1)	1.923(1)	1.923(1)	1.938(2)
1 ×	Mn2–O2	2.057(4)	2.053(5)	2.098(5)	2.067(6)	2.097(5)	2.088(6)
occ ×	Mn2–O3	1.701(3)	1.723(3)	1.706(3)			
	<Mn–O>	1.947(2)	1.945(2)	1.959(3)	1.952(3)	1.958(3)	1.968(3)
	V	3.05	3.02	2.98	3.01	2.98	2.91
% CO		77	72	66	74	70	62
$TbBaMn_2O_{5.5-y}$							
2 ×	Mn3–O4	1.903(1)	1.904(1)	1.906(2)	1.902(2)	1.902(2)	1.896(2)
	Mn3–O5	2.089(3)	2.091(3)	2.098(3)	2.100(3)	2.116(3)	2.133(4)
2 ×	Mn3–O6	1.940(6)	1.942(6)	1.945(6)	1.945(7)	1.948(7)	1.949(7)
occ ×	Mn3–O9	1.764(2)	1.774(2)	1.780(2)	1.784(3)		
	<Mn–O>	1.955(2)	1.956(2)	1.960(2)	1.958(2)	1.963(2)	1.965(2)
	V	3.01	2.98	2.96	2.99	2.95	2.95
2 ×	Mn4–O4	2.235(2)	2.236(2)	2.236(2)	2.240(2)	2.241(2)	2.247(2)
	Mn4–O5	1.901(3)	1.907(3)	1.900(3)	1.909(3)	1.903(3)	1.893(4)
2 ×	Mn4–O7	1.907(3)	1.908(3)	1.910(3)	1.910(3)	1.911(3)	1.914(3)
occ ×	Mn4–O8	1.899(2)	1.890(2)	1.894(3)	1.889(3)	1.891(3)	1.894(3)
	<Mn–O>	2.015(2)	2.015(2)	2.014(2)	2.020(2)	2.017(2)	2.018(2)
	V	3.22	3.24	3.26	3.23	3.25	3.25

[a]Linearly interpolated valeces are calculated as $V = [L(V_H–V_L)–(H–L)V_L]/[(V_H–V_L)–(H–L)]$, where Vn's are the BVSs calculated using parameters from ref. Twelve for the higher (H) and lower (L) formal oxidation states; here $H = 3$ and $L = 2$.

[b]$\%CO = 100\ (V_2-V_1)\ (F_H+F_L)/(V_2+V_1)\ (F_H-F_L)$, where F's are the formal site valences including allowance for excess oxygen, e.g. $F_L = 2.05$, $F_H = 3$ for $TbBaMn_2O_{5.025}$ at 100 °C.

in oxides has shown that the degree of CO is always reduced from the ideal value, typically to 20–80% of the ideal separation, so the values for $TbBaMn_2O_5$ are at the upper end of the observed range. The charge ordering transition temperature (T_{CO}), above which the translational symmetry between metal sites is restored, is <600 K in all other oxides but $TbBaMn_2O_5$ evidently has a remarkably high $T_{CO}>873$ K. In comparison to the structural analogues $TbBaFe_2O_5$ (38% CO, $T_{CO}=282$ K [14]), and $YBaCo_2O_5$ (71% CO, $T_{CO}=220$ K [15]), it is not evident why T_{CO} is so high for $TbBaMn_2O_5$, or why the %CO is relatively low for $TbBaFe_2O_5$, and further experimental and theoretical work on charge ordering will be needed to resolve these issues.

In conclusion, this experiment has shown that both the oxygen miscibility between $TbBaMn_2O_5$ and $TbBaMn_2O_{5.5}$, and T_{CO} for $TbBaMn_2O_5$, occur at unexpectedly high temperatures, above 600 °C. Further neutron diffraction studies at higher temperatures will therefore be needed to determine whether a topoelectronic relationship exists in this system, and to find the exceptionally high charge melting transition in $TbBaMn_2O_5$.

Acknowledgments

The authors thank Dr. Richard Ibberson, Dr. Jan-Willem Bos and Dr. Falak Sher for their assistance with collection of the neutron data and EPSRC for provision of neutron beam time. A.J.W. and J.P.A. acknowledge the Leverhulme Trust, and E.C.M acknowledges MEC, Spain, for support.

References

[1] J.P. Chapman, J.P. Attfield, M. Molgg, C.M. Friend, T.P. Beales, Angew. Chem. 35 (1996) 2482.
[2] F. Millange, E. Suard, V. Caignaert, B. Raveau, Mater. Res. Bull. 34 (1999) 109.
[3] F. Millange, V. Caignaert, B. Domenges, B. Raveau, Chem. Mater. 10 (1998) 1974.
[4] V. Caignaert, F. Millange, B. Domenges, B. Raveau, Chem. Mater. 11 (1999) 930.
[5] A.J. Williams, J.P. Attfield, Phys. Rev. B 66 (2002) 220405.
[6] T. Arima, D. Akahoshi, K. Oikawa, T. Kamiyama, M. Uchida, Y. Matsui, Y. Tokura, Phys. Rev. B 66 (2002) 140408.
[7] T. Nakajima, H. Kageyama, M. Ichihara, K. Ohoyama, H. Yoshizawa, Y. Ueda, J. Solid State Chem. 177 (2004) 987.
[8] A.J. Williams, J.P. Attfield, Phys. Rev. B 72 (2005) 024436.
[9] A.J. Williams, J.P. Attfield, S.A.T. Redfern, Phys. Rev. B 72 (2005) 184426.
[10] C. Perca, L. Pinsard-Gaudart, A. Daoud-Aladine, M. Fernandez-Diaz, J. Rodriguez-Carvajal, Chem. Mater. 17 (2005) 1835.
[11] A.C. Larson, R.B. Von Dreele, Los Alamos National Laboratory Report No. La-UR 86-748, 1987.
[12] N.E. Brese, M. O'Keeffe, Acta Crystallogr., Sect. B: Struct. Sci. B 47 (1991) 192.
[13] J.P. Attfield, Solid State Sci. 8 (2006) 861.
[14] P. Karen, P.M. Woodward, J. Linden, T. Vogt, A. Studer, P. Fischer, Phys. Rev. B 64 (2001) 214405.
[15] T. Vogt, P.M. Woodward, P. Karen, B.A. Hunter, P. Henning, A.R. Moodenbaugh, Phys. Rev. Lett. 84 (2000) 2969.